

Interconnect Modeling using a Surface Admittance Operator Derived with the Fokas Method

Dries Bosman¹, Martijn Huynen¹, Daniël De Zutter¹, Xiao Sun²,
Nicolas Pantano², Geert Van der Plas², Eric Beyne², Dries Vande Ginste¹

¹*Quest, IDLab, Department of Information Technology, Ghent University/imec, Ghent, Belgium*

²*imec, Leuven, Belgium*

dries.bosman@ugent.be

Abstract—In this contribution, we propose a novel approach to rigorously model interconnect structures with an arbitrary convex polygonal cross-section and general, piecewise homogeneous, material parameters. A full-wave boundary integral equation formulation is combined with a differential surface admittance approach, invoking an extended form of the numerically fast Fokas method to construct the pertinent operator. Several examples validate our method and demonstrate its applicability to per-unit-of-length resistance and inductance characterization.

Index Terms—differential surface admittance, Fokas method, interconnect modeling

I. INTRODUCTION

In our modern society, where information technology is omnipresent, the development of sophisticated devices at ever higher operating frequencies poses serious challenges, e.g., in terms of electromagnetic compatibility and signal integrity. Combined with the continuing miniaturization, this evolution renders a proper analysis of the occurring electromagnetic fields and their wave nature indispensable. More specifically, in high-frequency interconnects, phenomena such as the skin and proximity effect should be taken into account in a rigorous fashion. For electromagnetic solvers employing a volumetric mesh, such as the versatile finite elements method (FEM), the exponential nature of the current crowding enforces an intractably fine discretization. The boundary integral equation (BIE) method and many other surface-based techniques, on the other hand, require particular attention to deal with the numerical integration of the Green's function in highly conductive media [1].

A popular procedure to circumvent this strenuous situation replaces the conductive material by its surrounding medium, while introducing additional boundary conditions. For instance, in the class of approximate techniques, (local) surface impedances are invoked [2]. Alternatively, the differential surface admittance (DSA) operator [3] captures the substituted material's properties in an exact, global way. Its implementation requires the eigenfunctions of the considered cross-sections, imposing a *de facto* limitation to circular and rectangular shapes. An extension to triangles, not relying on the Dirichlet eigenfunctions, was presented in [4]. However, this approach involves special measures to eliminate a prominent Gibbs effect degrading the initial solution. Moreover, a combination of multiple triangular components is necessary

for the analysis of arbitrary polygonal cross-sections. In yet other formulations [6], numerical issues may arise, in particular in the case of high material contrasts [1].

Here, on the other hand, we invoke and extend the Fokas method [5] to construct the DSA operator, automatically expanding its applicability to arbitrary convex shapes, while combined magnetic and dielectric contrast is allowed. As such, our method can, e.g., account for etching effects during the manufacturing of integrated circuits, resulting in trapezoidal structures. Coupled with the discretized electric field integral equation (EFIE), a formalism to accurately characterize interconnect structures is obtained, even for high material contrast and a strongly developed skin effect.

II. FORMULATION OF THE METHOD

Consider the two-dimensional (2-D) transverse magnetic (TM) polarized electromagnetic regime with a $e^{j\omega t}$ time dependence. We study a polygonal cylinder (typically a conductor) with M corner points (x_m, y_m) in the xy -plane, denoted as complex numbers $\zeta_m = x_m + jy_m$. The cylinder is characterized by its permittivity ϵ_i , permeability μ_i , conductivity σ_i and wavenumber k_i , and is situated in a homogeneous background medium with material properties ϵ_e , μ_e , σ_e and wavenumber k_e , as depicted in Fig. 1(a). Its longitudinal dimension is aligned with the z -axis. By applying the single source equivalence theorem, introducing an equivalent surface current density $\mathbf{j}_s = j_{s,z}\hat{\mathbf{z}}$ on the boundary \mathcal{C} , we can replace the cylinder's material by its surrounding medium, preserving the outside fields, while the inside fields $(\mathbf{e}_i, \mathbf{h}_i)$ are modified to the fictitious quantities $(\mathbf{e}'_i, \mathbf{h}'_i)$, as in Fig. 1(b). This equivalent surface current density is given by

$$\mathbf{j}_s = \hat{\mathbf{n}} \times (\mathbf{h}_i - \mathbf{h}'_i). \quad (1)$$

At the boundary of the structure, and only there, we find that $\mathbf{e}_i = \mathbf{e}'_i \triangleq \mathbf{e} = e_z\hat{\mathbf{z}}$, which is mapped to its normal derivative in the original and the equivalent situation via Dirichlet-to-Neumann (DtN) operators \mathcal{X} and \mathcal{X}' , resp.:

$$-j\omega\mu_i(\hat{\mathbf{n}} \times \mathbf{h}_i) = \mathcal{X}\mathbf{e}, \quad (2)$$

$$-j\omega\mu_e(\hat{\mathbf{n}} \times \mathbf{h}'_i) = \mathcal{X}'\mathbf{e}. \quad (3)$$

By combining (1), (2) and (3), we obtain

$$\mathbf{j}_s = \left(\frac{\mathcal{X}'}{j\omega\mu_e} - \frac{\mathcal{X}}{j\omega\mu_i} \right) \mathbf{e} \triangleq \mathcal{Y}\mathbf{e}, \quad (4)$$

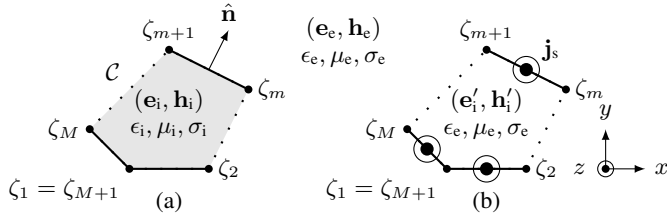


Fig. 1: Geometry of the problem, illustrating the equivalence theorem, with (a) the original and (b) the equivalent situation.

where \mathcal{Y} is the desired DSA operator [3].

The tangential electric field e_z satisfies the Helmholtz equation with eigenvalues k_i and k_e :

$$\nabla^2 e_z + k_{\{i,e\}} e_z = 0. \quad (5)$$

To solve the boundary value problems posed by (2), (3) and (5) we propose a Fokas-like method [5]. The following Fourier transform, the so-called global relation, is at its core:

$$F(\lambda) = \int_C \exp \left[-\frac{j k}{2} \left(\frac{\tilde{\zeta}}{\lambda} + \lambda \zeta \right) \right] \times \left[\frac{k \phi}{2} \left(\lambda d\zeta - \frac{d\tilde{\zeta}}{\lambda} \right) + \frac{\partial \phi}{\partial n} d\zeta \right] = 0, \quad \forall \lambda \in \mathbb{C}, \quad (6)$$

where $\zeta_m = x_m + jy_m$, $\tilde{\cdot}$ indicates the complex conjugate and \mathcal{C} denotes the polygonal boundary. Furthermore, $\phi = e_z$ and $\frac{\partial \phi}{\partial n} = -j\omega\mu_{\{i,e\}} h_{\tan}^{\{i,e\}}$ in our case. Equation (6) is cast onto an appropriate basis of P orthogonal Legendre polynomials on each polygon side and evaluated at Λ well-chosen spectral collocation points $\lambda \in \mathbb{C}$:

$$\lambda = -\frac{l/k + \sqrt{(l/k)^2 - |h_m|^2}}{h_m}, \quad (7)$$

for $l \in \{0, 1, 2, \dots, \Lambda - 1\}$ and $m \in \{1, 2, \dots, M\}$, where $h_m = (\zeta_{m+1} - \zeta_m)/2$ and k is the wavenumber. This way, one ends up with an overdetermined, but very quickly solved, linear system with a solution that finally yields a discrete approximation of the pertinent DtN operators.

To incorporate this result in a BIE framework, a transformation to local, pulse-shaped basis functions is performed. By collecting the corresponding expansion coefficients of \mathbf{j}_s and \mathbf{e} into vectors \mathbf{J} and \mathbf{E} , we obtain the discretized version of (4):

$$\overline{\overline{\mathbf{G}}}\mathbf{J} = \left(\frac{\overline{\overline{\mathbf{X}}'}}{j\omega\mu_e} - \frac{\overline{\overline{\mathbf{X}}}}{j\omega\mu_i} \right) \mathbf{E} \triangleq \overline{\overline{\mathbf{Y}}}\mathbf{E}, \quad (8)$$

with $\overline{\overline{\mathbf{G}}}$ the Gram matrix of the local basis functions.

To find the per-unit-of-length (p.u.l.) resistance and inductance matrices $\overline{\overline{\mathbf{R}}}$ and $\overline{\overline{\mathbf{L}}}$ for a configuration with N conductors, we invoke the procedure outlined in [3], yielding

$$\overline{\overline{\mathbf{R}}} + j\omega\overline{\overline{\mathbf{L}}} = \left(\overline{\overline{\mathbf{T}}}^T \left(\overline{\overline{\mathbf{G}}}\overline{\overline{\mathbf{Y}}}^{-1}\overline{\overline{\mathbf{G}}} + j\omega\overline{\overline{\mathbf{A}}} \right)^{-1} \overline{\overline{\mathbf{T}}} \right)^{-1}, \quad (9)$$

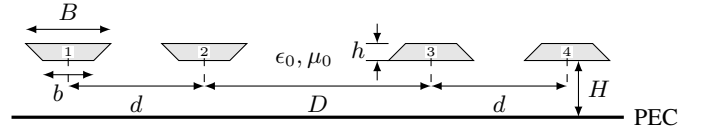
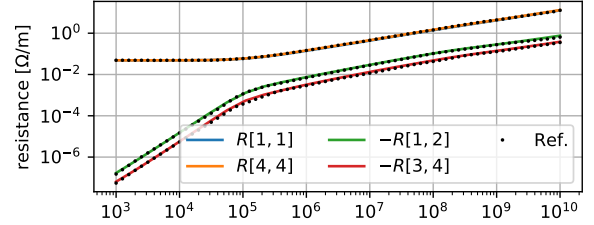
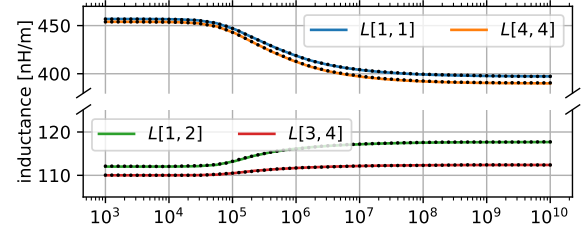


Fig. 2: Configuration with four trapezoidal conductors ($\sigma = 5.72 \times 10^7$ S/m) with dimensions in mm: $B = 1.5$, $b = 0.9$, $h = 0.3$, $D = 4$, $d = 2.4$ and $H = 1.5$, situated above an infinite PEC ground plane.



(a) Pu.l. resistance in Ω/m .



(b) Pu.l. inductance in nH/m.

Fig. 3: Relevant elements of the resistance and inductance matrices $\overline{\overline{\mathbf{R}}}$ and $\overline{\overline{\mathbf{L}}}$, for the configuration of Fig. 2.

where the elements of the matrix $\overline{\overline{\mathbf{A}}}$ are obtained through

$$\left(\overline{\overline{\mathbf{A}}} \right)_{ij} = -\mu_e \int_C \int_{C'} G(\mathbf{r}, \mathbf{r}') b_i(c) b_j(c') dc' dc. \quad (10)$$

with $G(\mathbf{r}, \mathbf{r}') = \ln |\mathbf{r} - \mathbf{r}'| / (2\pi)$, the 2-D static Green's function. The matrix $\overline{\overline{\mathbf{T}}}$ is defined as

$$\left(\overline{\overline{\mathbf{T}}} \right)_{in} = \begin{cases} \ell_i, & \text{if segment } i \in \text{conductor } n \\ 0, & \text{otherwise,} \end{cases} \quad (11)$$

with ℓ_i the length of segment i in the mesh.

III. NUMERICAL EXAMPLES

Consider the configuration with two oppositely oriented trapezoidal line pairs and conductivity $\sigma = 5.72 \times 10^7$ S/m above an infinite ground plane, shown with annotated dimensions in Fig. 2. Relevant elements of the corresponding resistance matrix $\overline{\overline{\mathbf{R}}}$ and inductance matrix $\overline{\overline{\mathbf{L}}}$, determined by means of the procedure outlined above, are compared to the reference solution provided by [4] in Fig. 3. The pertinent system matrix is constructed invoking $P = 20$ Legendre polynomials per side of the trapezoids, and is evaluated in $\Lambda = 40$ collocation points λ per side as well. These values for the parameters (P, Λ) will also be utilized in the remaining examples. An excellent agreement between our proposed method and the result found in literature is observed.

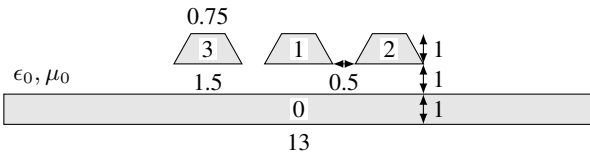


Fig. 4: Multiconductor transmission line ($\sigma = 3.57 \times 10^7$ S/m) with three trapezoidal signal lines and a finite rectangular reference conductor. All dimensions are in μm .

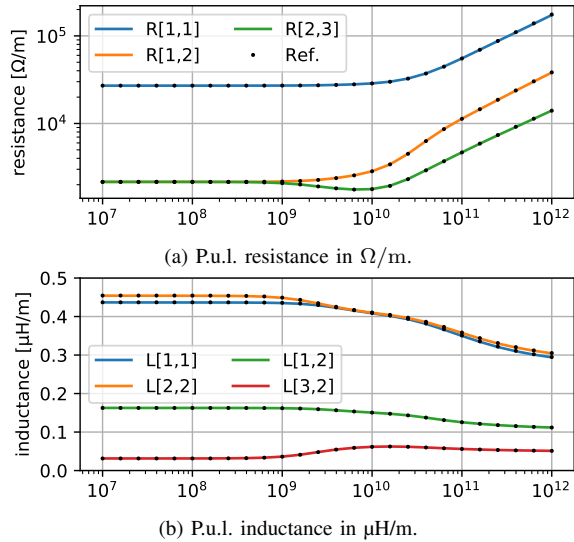


Fig. 5: Relevant elements of the resistance and inductance matrices $\overline{\overline{R}}$ and $\overline{\overline{L}}$, for the configuration of Fig. 4.

Next, we study the multiconductor transmission line depicted in Fig. 4, with reference conductor 0. The dimensions annotated on the figure are all given in μm . We obtain the curves plotted in Fig. 5, validated by means of the results in [6]. Once again, both sets of results match excellently.

Finally we investigate the influence of the conductor ($\sigma = 1 \times 10^7$ S/m, $\mu_r = 5$) shape in the configuration of Fig. 6, evolving from triangular (solid lines), over asymmetric trapezoidal (dashed) to rectangular (dotted). This example includes a conductive, magnetic medium and therefore demonstrates the capability of our method to model this novel class of materials, present in state-of-the-art interconnect applications [7]. The elements of the matrices $\overline{\overline{R}}$ and $\overline{\overline{L}}$ are given in Fig. 7, for these three shapes. Note that $R_{11} = R_{22}$ and $L_{11} = L_{22}$ owing to the symmetry of our problem.

For all of the above examples, the calculation of the DSA matrix by means of a Python code on a system with a 1.9GHz CPU and 16GB of RAM required less than 0.5s per frequency point, a value comparable to the times reported in [6], confirming the efficiency of our method.

IV. CONCLUSIONS

We presented a novel interconnect modeling technique, combining a boundary integral equation framework with a differential surface admittance operator, constructed through application of the numerically fast Fokas method. Our approach

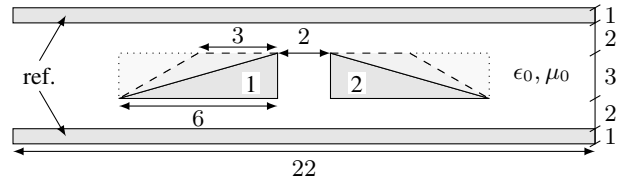


Fig. 6: Multiconductor transmission line ($\sigma = 1 \times 10^7$ S/m, $\mu_r = 5$) with two triangular/trapezoidal/rectangular signal lines and two finite rectangular reference conductors. All dimensions are in 0.1 mm.

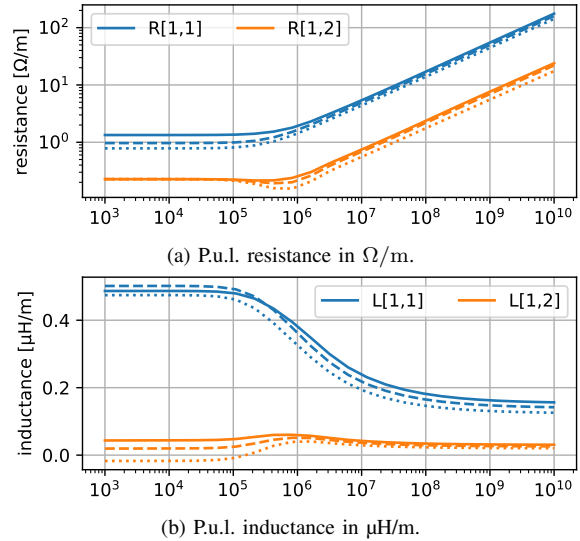


Fig. 7: Relevant elements of the resistance and inductance matrices $\overline{\overline{R}}$ and $\overline{\overline{L}}$, for the configuration of Fig. 6. The solid, dashed and dotted lines correspond to the triangular, trapezoidal and rectangular conductor shapes, resp.

supports multiconductor configurations with arbitrary, piecewise homogeneous material properties and convex polygonal shapes. By means of per-unit-of-length resistance and inductance characterization of these structures, we demonstrated our method's accuracy, efficiency and broadband applicability.

REFERENCES

- [1] J. Peeters, I. Bogaert, and D. De Zutter, "Calculation of MoM interaction integrals in highly conductive media," *IEEE Trans. Antennas Propag.*, vol. 60, no. 2, pp. 930–940, Feb 2012.
- [2] T. B. A. Senior, and J. L. Volakis, "Approximate boundary conditions in electromagnetics," Institution of Electrical Engineers, 1995.
- [3] D. De Zutter, and L. Knockaert, "Skin effect modeling based on a differential surface admittance operator," *IEEE Trans. Microw. Theory Techn.*, vol. 53, no. 8, pp. 2526–2538, Aug 2005.
- [4] T. Demeester, and D. De Zutter, "Construction of the Dirichlet to Neumann boundary operator for triangles and applications in the analysis of polygonal conductors," *IEEE Trans. Microw. Theory Techn.*, vol. 58, no. 1, pp. 116–127, Jan 2010.
- [5] A. S. Fokas, N. Flyer, S. A. Smitheman, and E. A. Spence, "A semi-analytical numerical method for solving evolution and elliptic partial differential equations," *J. Comput. Appl. Math.*, vol. 227, no. 1, pp. 59–74, May 2009.
- [6] U. R. Patel and P. Triverio, "Skin effect modeling in conductors of arbitrary shape through a surface admittance operator and the contour integral method," *IEEE Trans. Microw. Theory Techn.*, vol. 64, no. 9, pp. 2708–2717, Sept 2016.
- [7] N. A. Lanzillo *et al.*, "Exploring the limits of cobalt liner thickness in advanced copper interconnects," *IEEE Electron Device Lett.*, vol. 40, no. 11, pp. 1804–1807, Nov 2019.